Eur. Phys. J. C (2023) 83:14
https://doi.org/10.1140/epjc/s10052-022-11148-5

THE EUROPEAN PHYSICAL JOURNAL C

Regular Article - Theoretical Physics

Bremsstrahlung as a probe of baryon stopping in heavy-ion collisions

Sigurd Nese[a], **Joakim Nystrand**[b]

Department of Physics and Technology, University of Bergen, Bergen, Norway

Received: 2 November 2022 / Accepted: 20 December 2022 / Published online: 11 January 2023

Abstract In collisions between heavy ions at ultra-relativistic energies the participating protons lose energy, which is converted into new particles. As the protons slow down, they emit bremsstrahlung radiation. The yield and angular distribution of the emitted radiation are sensitive probes of how much energy the incoming protons have lost. In this paper, the spectrum of bremsstrahlung radiation is calculated for different stopping scenarios, and the results are compared with the expected yield of photons from hadronic interactions.

1 Introduction

In collisions between heavy ions at relativistiv energies there is convincing evidence that a new state of matter, a quark–gluon plasma, is formed [1]. In this state, the quarks and gluons are no longer confined to nucleons but can move freely over distances large compared with the size of a single nucleon. The energy density in the quark gluon plasma formed in Pb + Pb collisions at the LHC has been estimated from measurements of the total transverse energy at midrapidity to be on the order of 12–14 GeV/fm^3 at a time of 1 fm/c after the collision [2,3]. This is far above the densitites of 0.2–0.5 GeV/fm^3 lattice QCD calculations find are required for deconfinement [4].

The energy deposited in the quark–gluon plasma comes from the energy lost by the incoming nuclei, and one of the most fundamental question one can address in the study of high energy heavy-ion collisions is therefore how much energy the incoming baryons lose. This is usually referred to as the amount of baryon stopping. One can have scenarios ranging from complete stopping, where the incoming baryons lose all their energy, to full transparency, where the baryons lose no or very little energy. Full stopping would imply that all baryons end up close to midrapidity, whereas full transparency would leave the baryons near beam rapidity. Since baryon number is conserved, the fate of the baryons in the colliding nuclei can be determined from the rapidity distribution of net baryons, that is $dn_B/dy - dn_{\overline{B}}/dy$. For experimental reasons, one is often restricted to study the net proton rather than the net baryon distributions.

Results from the Relativistic Heavy-Ion Collider (RHIC) [5–7] and fixed target experiments at the CERN SPS [8] show that the amount of stopping decreases with increasing collision energy in the range $\sqrt{s_{NN}} = 7$–200 GeV. There have been attempts to explain the energy loss in this energy range from hadron transport models [9] and models based on the Color Glass Condensate [10,11].

At the CERN SPS and RHIC, identified protons and antiprotons could be measured down to low transverse momenta $p_T \sim 0$ over a wide rapidity range, and the net-proton rapidity distributions could thus be determined. Such measurements were performed by the NA49 [8] and BRAHMS [6,7] experiments. At the LHC, the situation is different. The only experiment which has measured identified protons and antiprotons at low p_T is ALICE. The results have shown that in the central rapidity region $|y| \leq 0.5$ there are no net protons [12–14]. But beyond that, there are no experimental constraints on how the net-protons are distributed.

To improve this situation, we propose to use the bremsstrahlung photons emitted when the nuclei slow down. This idea was first suggested before the start of the relativistic heavy-ion programs at CERN and RHIC [15,16]. Before the start-up of RHIC, several studies were made where this process was considered [17–19]. These also included a proposal to build a dedicated detector to study this radiation [18], but those plans were never realized. Recently, the idea was brought up again in the context of the LHC [20].

[a] e-mail: sigun@uio.no

[b] e-mail: Joakim.Nystrand@uib.no (corresponding author)

The previous studies mentioned above all use a similar, semi-classical approach to calculate the bremsstrahlung spectrum, based on the description in [21]. Our calculations will follow the same path. We will, however, implement improved stopping scenarios which are either based on model calculations or phenomenological and consistent with existing data. The stopping scenarios considered in [20] are simplified and do not take into account the fact that the central region ($|y| \leq 0.5$) at the LHC is baryon free. This was, however, recently followed up by a study of phenomenological stopping scenarios where the central region is almost baryon free [22].

We will also, for the first time, make a detailed estimate of the background from hadronically produced photons, primarily from the decay of π^0 mesons. This background is obtained from simulations with PYTHIA 8.3 [23]. The goal is to determine in what regions of phase space one can expect bremsstrahlung photons to provide a realistic measure of the nuclear stopping. One can, in addition to photons from hadronic interactions, also expect a large background from secondary photons produced in the detector material. The latter is specific to a certain experiment and its material budget and is thus beyond the scope of this paper.

2 The bremsstrahlung spectrum

The energy radiated per solid angle from a current $\mathbf{J}(\mathbf{r}, t)$ is given by [21]

$$\frac{d^2I}{d\omega d\Omega} = \frac{\omega^2}{4\pi^2}\left|\int\int \overline{n}\times(\overline{n}\times\mathbf{J}(\mathbf{r},t))e^{i\omega(t-\overline{n}\cdot\mathbf{r}(t))}dtd^3\mathbf{r}\right|^2. \tag{1}$$

The vector $\overline{n}$ is a unit vector in the direction of the photon, and here and throughout we use units where $\hbar = c = 1$. We choose coordinates where the incoming beams move along the z-axis and the photon is emitted in the xz-plane with angle θ, giving $\overline{n} = (\sin(\theta), 0, \cos(\theta))$.

In the center of mass, the incoming nuclei are Lorentz contracted in the longitudinal direction to a size $\sim R/\gamma$, where R is the nuclear radius and γ the Lorentz factor of the beam. For a lead nucleus at the LHC, this corresponds to a longitudinal size of about 0.003 fm. It is thus justified to ignore the longitudinal relative to the transverse extension and write the currents for the incoming nuclei as

$$\begin{aligned}\mathbf{J}_+(\mathbf{r},t) &= +v_0\tfrac{e}{\sqrt{4\pi\epsilon_0}}\sigma(r_\perp)\delta(z-v_0t)\,\theta(-t)\hat{\mathbf{z}}\\ \mathbf{J}_-(\mathbf{r},t) &= -v_0\tfrac{e}{\sqrt{4\pi\epsilon_0}}\sigma(r_\perp)\delta(z+v_0t)\,\theta(-t)\hat{\mathbf{z}}\,.\end{aligned} \tag{2}$$

Here, σ is the nuclear electric charge density in the transverse plane, v_0 the velocity, $v_0 = \tanh(y_b)$, where y_b is the beam rapidity, and $\theta(t)$ the Heaviside step function. The charge density is normalized to $\int \sigma d^2\mathbf{r}_\perp = Z$, where Z is the number of protons in the beam nucleus. The outgoing protons will have a distribution in the transverse plane, which we assume is the same as for the incoming particles, and a distribution in velocities, which may or may not depend on the position in the transverse plane. Writing the velocity in terms of the rapidity, $v(y) = \tanh(y)$, and the corresponding density as $\rho(y, r_\perp)$ one gets for the outgoing current

$$\mathbf{J}_f(\mathbf{x},t) = \sigma(r_\perp)\frac{e}{\sqrt{4\pi\epsilon_0}} \int_{-\infty}^{+\infty}\rho(r_\perp, y)v(y)\delta(z-v(y)t)dy\,\theta(t)\hat{\mathbf{z}}. \tag{3}$$

The density of the outgoing protons is normalized to

$$\int_{-\infty}^{+\infty}\rho(r_\perp, y)dy = 2, \tag{4}$$

since it includes the contribution from both incoming nuclei. With the total current $\mathbf{J} = \mathbf{J}_+ + \mathbf{J}_- + \mathbf{J}_f$, the radiated energy becomes

$$\begin{aligned}\frac{d^2I}{d\omega d\Omega} = \frac{\omega^2}{4\pi^2}\Big|&\int\int \overline{n}\times(\overline{n}\times\mathbf{J}_+(\mathbf{r},t))e^{i\omega(t-\overline{n}\cdot\mathbf{r}(t))}dtd^3\mathbf{r}\\ &+\int\int \overline{n}\times(\overline{n}\times\mathbf{J}_-(\mathbf{r},t))e^{i\omega(t-\overline{n}\cdot\mathbf{r}(t))}dtd^3\mathbf{r}\\ &+\int\int \overline{n}\times(\overline{n}\times\mathbf{J}_f(\mathbf{r},t))e^{i\omega(t-\overline{n}\cdot\mathbf{r}(t))}dtd^3\mathbf{r}\Big|^2.\end{aligned} \tag{5}$$

Integrating by parts in the integral over time one obtains

$$\begin{aligned}&\frac{d^2I}{d\omega d\Omega}\\ &= \frac{\omega^2}{4\pi^2}\Big|\frac{1}{i\omega}\int\left[\int\frac{d}{dt}\left[\frac{\overline{n}\times(\overline{n}\times\mathbf{J}_+(\mathbf{r},t))}{1-\overline{n}\cdot\dot{\mathbf{r}}(t)}\right]e^{i\omega(t-\overline{n}\cdot\mathbf{r}(t))}dt\right]d^3\mathbf{r}\\ &+\frac{1}{i\omega}\int\left[\int\frac{d}{dt}\left[\frac{\overline{n}\times(\overline{n}\times\mathbf{J}_-(\mathbf{r},t))}{1-\overline{n}\cdot\dot{\mathbf{r}}(t)}\right]e^{i\omega(t-\overline{n}\cdot\mathbf{r}(t))}dt\right]d^3\mathbf{r}\\ &+\frac{1}{i\omega}\int\left[\int\frac{d}{dt}\left[\frac{\overline{n}\times(\overline{n}\times\mathbf{J}_f(\mathbf{r},t))}{1-\overline{n}\cdot\dot{\mathbf{r}}(t)}\right]e^{i\omega(t-\overline{n}\cdot\mathbf{r}(t))}dt\right]d^3\mathbf{r}\Big|^2.\end{aligned} \tag{6}$$

The time, Δt, and longtudinal distance over which the protons are slowed down can be expected to be small compared with the transverse size, $\Delta t << R$. For low energy photons ($\omega << 1/\Delta t$), it is therefore justified to neglect the time and longitudinal components in the phase factor and make the assupmtion

$$e^{i\omega(t-\overline{n}\cdot\mathbf{r})} \approx e^{-i\omega x\sin(\theta)}. \tag{7}$$

With these assumptions the integrals over time and z in (6) can be performed, leading to

$$\frac{d^2I}{d\omega d\Omega} = \frac{\alpha}{4\pi^2}\sin^2(\theta)\left|\int \sigma(r_\perp)e^{i\omega x\sin(\theta)} - \left[\int \frac{v(y)}{1-v(y)\cos(\theta)}\rho(y,r_\perp)dy \frac{2v_0^2\cos(\theta)}{1-v_0^2\cos^2(\theta)}\right]d^2r_\perp\right|^2. \quad (8)$$

Here, $\alpha = e^2/4\pi\epsilon_0$ is the fine structure constant. This result is in agreement with [18]. To do the integral over the transverse dimensions, one has to know the function $\rho(y, r_\perp)$. It is conceivable that there is a dependence of the rapidity loss of the protons on the transverse coordinate; protons close to the center of the nuclei can be expected to lose more energy than those on the periphery. Previous studies have, however, found that the dependence of $\rho(y, r_\perp)$ on the transverse position has only a minor effect on the spectrum of bremsstrahlung photons [18,19]. Moreover, the models we will use for the rapidity loss of the protons provide the average loss, independent of position in the transverse plane. We will therefore ignore the dependence on $r_\perp$ here and assume $\rho(y, r_\perp) = \rho(y)$. The integral over $r_\perp$ can then be performed and the spectrum of emitted photons can be written

$$\frac{dN_\gamma}{d\omega d\Omega} = \frac{\alpha Z^2}{4\pi^2\omega}\sin^2(\theta)|F(\omega\sin(\theta))|^2 \left[\int \frac{v(y)\rho(y)}{1-v(y)\cos(\theta)}dy - \frac{2v_0^2\cos(\theta)}{1-v_0^2\cos^2(\theta)}\right]^2. \quad (9)$$

Here, $F(Q)$ is the nuclear form factor obtained from a Fourier transform of the nuclear charge distribution, ρ_A:

$$F(Q) = \frac{1}{Z}\int \rho_A(\mathbf{r})e^{-i\mathbf{q}\cdot\mathbf{r}}d^3\mathbf{r} \approx \frac{1}{Z}\int \sigma(r_\perp)e^{-i\omega x\sin(\theta)}d^2r_\perp. \quad (10)$$

We use a form factor

$$F(Q) = \frac{4\pi\rho_0}{AQ^3}(\sin(QR_A) - QR_A\cos(QR_A))\left[\frac{1}{1+a^2Q^2}\right], \quad (11)$$

where $R_A = 6.62$ fm, $\rho_0 = 0.161$ fm^{-3}, and $a = 0.70$ fm for a Pb nucleus. This parameterization has been shown to reproduce the Fourier transform of a Woods–Saxon distribution in configuration space very well [24].

One can note that for low energy photons and small emission angles, $\omega\sin(\theta) << 1/R$, the Form Factor in Eq. 9 is approximately 1. The energy and angular dependencies then factorize, with the energy dependence given by $1/\omega$ and the angular dependence by

$$\frac{dN_\gamma}{d\theta} \propto \sin^3(\theta)\left[\int \frac{v(y)\rho(y)}{1-v(y)\cos(\theta)}dy - \frac{2v_0^2\cos(\theta)}{1-v_0^2\cos^2(\theta)}\right]^2. \quad (12)$$

To proceed with the calculations one has to define the function $\rho(y)$, the rapidity distribution of the net-protons in the final state. We consider 3 scenarios for central Pb + Pb collisions at the LHC.

1. The net proton distribution as given by PYTHIA 8.3 [23]. Heavy-ion collisions have been implemented in PYTHIA through the Angantyr model [25]. The scaling from proton-proton collisions is based on the Glauber model and the original PYTHIA framework is used to describe the individual nucleon–nucleon sub-collisions. It thus extrapolates the dynamics of pp collisions to heavy-ion collisions, without introducing any collective effects between the nucleon–nucleon collisions. It does reproduce the measured charged particle pseudorapidity distributions in Pb + Pb collisions at the LHC.
2. The net proton distribution as given by the hadron transport model SMASH-2.2 [9,26]. The model combines a string model, where the colliding hadrons are excited to strings which fragment, with elastic and inelastic interaction between hadrons in the later stages of the collisions. This approach leads to a considerably larger amount of stopping compared with PYTHIA. In fact, the model predicts a non-zero number of net-protons at midrapidity. We use this result for the current calculation anyway, since it represents a valid result of the model at LHC energies [H. Elfner, private communication].
3. A phenomenological model where the central region, $|y| \leq 0.5$, contains no net protons, but where the protons have a considerable shift away from beam rapidity. This is modelled by the sum of two skewed Gaussians.

The net-proton rapidity distributions, $\rho(y)$, for these 3 scenarios are shown in Fig. 1. Of the three models, Pythia clearly shows the least amount of stopping. While SMASH-2.2 exhibits a non-zero yield of net-protons at midrapidity, the protons are on average not shifted so much toward $y = 0$ as in scenario 3.

3 Results

The angular distributions of bremsstrahlung photons in the forward direction, integrated over the energy range $0.1 \leq \omega \leq 0.5$ GeV, from the 3 scenarios are shown in Fig. 2a). The distributions are peaked close to $1/\gamma$, as expected, and

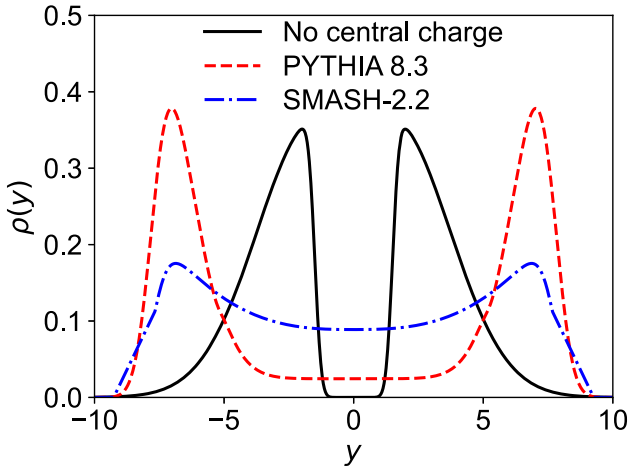

Fig. 1 Net-proton rapidity distributions for the 3 scenarios described in the text

the yields increase with an increasing amount of stopping. The curves also exhibit different angular dependencies, the scenarios with more stopping having more persistent tails toward larger angles. Thus, the models are differentiated in both total photon yield and angular dependence.

To facilitate a comparison with experimental acceptances, which are usually defined in terms of pseudorapidity, $\eta = -\ln(\tan(\theta/2))$, the angular distribution in Eq. 9 can be rewritten as

$$\frac{dN_\gamma}{d\omega d\eta d\phi} = \frac{dN_\gamma}{d\omega d\Omega}\sin^2(\theta). \tag{13}$$

The pseudorapidity distribution, integrated over azimuthal angle and energy interval $0.1 \le \omega \le 0.5$ GeV, is shown in Fig. 2b. The difference between the spectra is more pronounced in the pseudorapidity distribution than in the angluar distribution. This is due to the factor $\sin^2\theta = 1/\cosh^2(\eta)$ which varies rapidly for large $|\eta|$. Covering the entire range of emission angles, the figure illustrates the difference in total number of radiated photons between the stopping scenarios. Furthermore, while the peaks of all three spectra lie at large pseudorapidities, the scenarios give significantly differing photon yields at lower η as well, making such scenarios potentially discernable within experimental acceptances.

To put these numbers in context, we compare them with the photon yield from the 5% most central Pb + Pb collisions from PYTHIA 8.3 in Fig. 3. These hadronically produced photons, most of which come from the deacy $\pi^0 \to \gamma + \gamma$, constitute a background to the bremsstrahlung photons we are considering here. The background yield is shown by the black histograms in the figure. The sum of the yield of the background and bremsstrahlung photons is shown by the solid, blue histograms for scenario 1–3 in Fig. 3a–c, respectively. The number of bremsstrahlung photons is calculated from

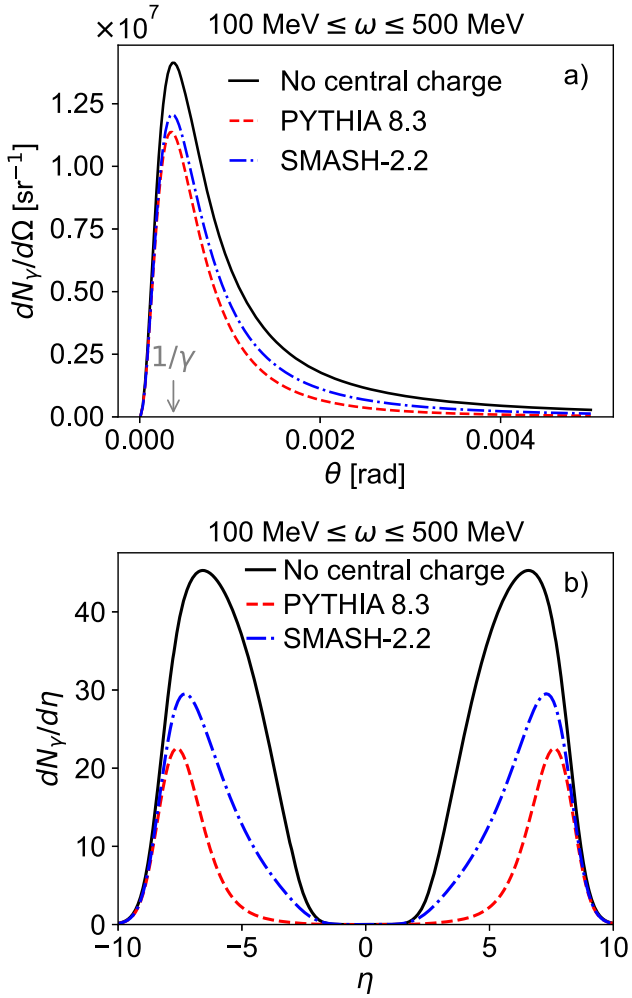

Fig. 2 **a** The angular distribution of bremsstrahlung photons with energies between $0.1 \le \omega \le 0.5$ GeV for the 3 scenarios. **b** The pseudorapidity distributions, $dN_\gamma/d\eta$, of bremsstrahlung photons within the same energy range

Eq. 13, integrated over azimuthal angle and photon energy $0.1 \le \omega \le 0.5$ GeV.

The bremsstrahlung calculations above assume that all protons participate in the collision. This will not be the case for collisions within a finite impact parameter range. We therefore calculate a correction factor $(\langle N_{p,\,\mathrm{part}}\rangle/2Z)^2$, where $\langle N_{p,\,\mathrm{part}}\rangle = 151$ is the average number of participating protons in the 5% most central collisions in Pythia. The result of applying this correction factor to the yield of bremsstrahlung photons is shown by the dashed, blue histograms in the figure.

From the figure one can see that at low pseudorapidities, the background completely dominates. In the very forward direction, however, the background falls off quickly while the bremsstrahlung peak emerges. The yield of bremsstrahlung photons differ widely between the different scenarios, which emphasizes that this is indeed a very sensitive probe of the

amount of nuclear stopping. The shapes of the pseudorapidity distributions are also quite different between the scenarios. This means that the limit in pseudorapidity where one can expect a significant signal over background is lower the larger amount of stopping one has.

As mentioned, a detailed discussion of in which experiments one might extract a bremsstrahlung signal is beyond the scope of this paper. We nevertheless indicate in Fig. 3 the experimental acceptances of the current and future experiments where it might be possible. The existing LHCb experiment has an electromagnetic calorimeter coverage between $2.0 \leq \eta \leq 4.5$ [27]. We include it here, although it might not be able to reach low enough photon energies at large pseudorapidities [28, R. McNulty, private communication]. During the Next Long Shutdown at the LHC (2026–2029) it is foreseen to install a forward calorimeter (FoCal) in the ALICE experiment [29]. It will consist of a high resolution electromagnetic and hadronic calorimeter covering $3.4 \leq \eta \leq 5.8$. Finally, beyond LHC Run 4 there are plans to upgrade the ALICE experiment to ALICE-3 [30]. The current design of ALICE-3 includes a Forward Conversion Tracker, which should have the possibility to measure photons with energies down to or below 100 MeV in the pseudorapidity range $3.0 \leq \eta \leq 5.0$. The pseudorapidity coverages of these detectors are shown by the red lines in Fig. 3.

From the figure one can see that for scenario 3, "No central charge", there is a visible excess over the hadronic background within the pseudorapidity coverage of all the detectors mentioned above. For scenario 1, "PYTHIA 8.3", the situation is less favorable and one would have to go to the most forward regions of ALICE-3 and FoCal to find a good signal to background ratio.

Since the Photon Conversion Tracker in ALICE-3 aims at measuring photons with energies below 100 MeV, we also include a plot of the photon pseudorapidity distributions for the photon energy range $0.01 \leq \omega \leq 0.1$ GeV in Fig. 4. In this energy range, there is a significant excess inside the ALICE-3 acceptance for all stopping scenarios.

In addition to being peaked in the forward direction, the bremsstrahlung spectrum increases rapidly with decreasing photon energy, approximately as $1/\omega$, as was mentioned above. This is contrary to the background from hadronically produced photons, which decrease with decreasing ω in the energy range considered here. To illustrate this, we plot the energy spectrum integrated over azimuthal angle and pseudorapidity range $4 \leq \eta \leq 5$ in Fig. 5. As in Figs. 3 and 4, the background is given by the black histograms, and the uncorrected and corrected signal plus background by the solid and dashed blue histograms, respectively. As for the pseudorapidity distributions, the energy below which one can expect a significant signal over background is highly dependent on the stopping scenario. Also the yield is strongly dependent on the stopping scenario.

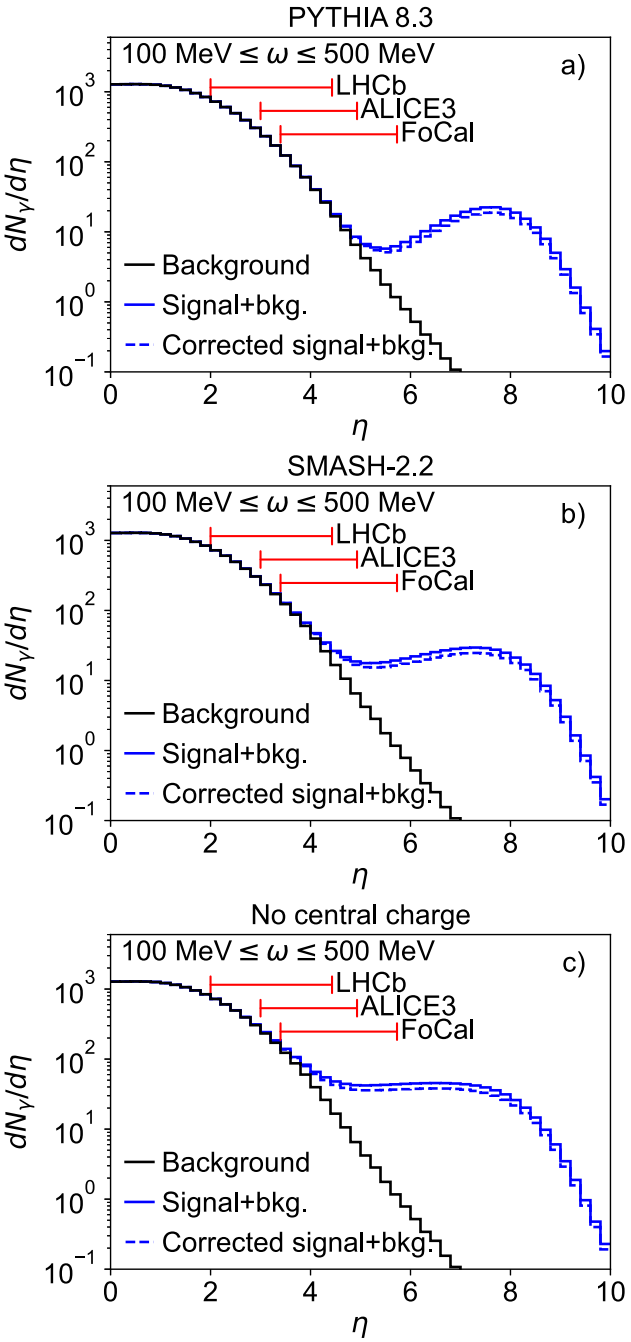

Fig. 3 The pseudorapidity distributions for photons with $0.1 \leq \omega \leq 0.5$ GeV integrated over the azimuthal angle. The black histogram shows the background from hadronically produced photons. The solid blue histogram shows the sum of the photons from bremsstrahlung radiation and hadronic production. The correction applied to the bremsstrahlung spectrum to obtain the dashed blue histogram is described in the text

The inset in Fig. 5a shows the low energy region, and it emphasizes that if one can go to low enough photon energies, a signal will be visible also in scenarios with a small amount of stopping. One should keep in mind that it might be possible to extract a bremsstrahlung signal, even with a rather low signal to background ratio, by subtracting the hadronic

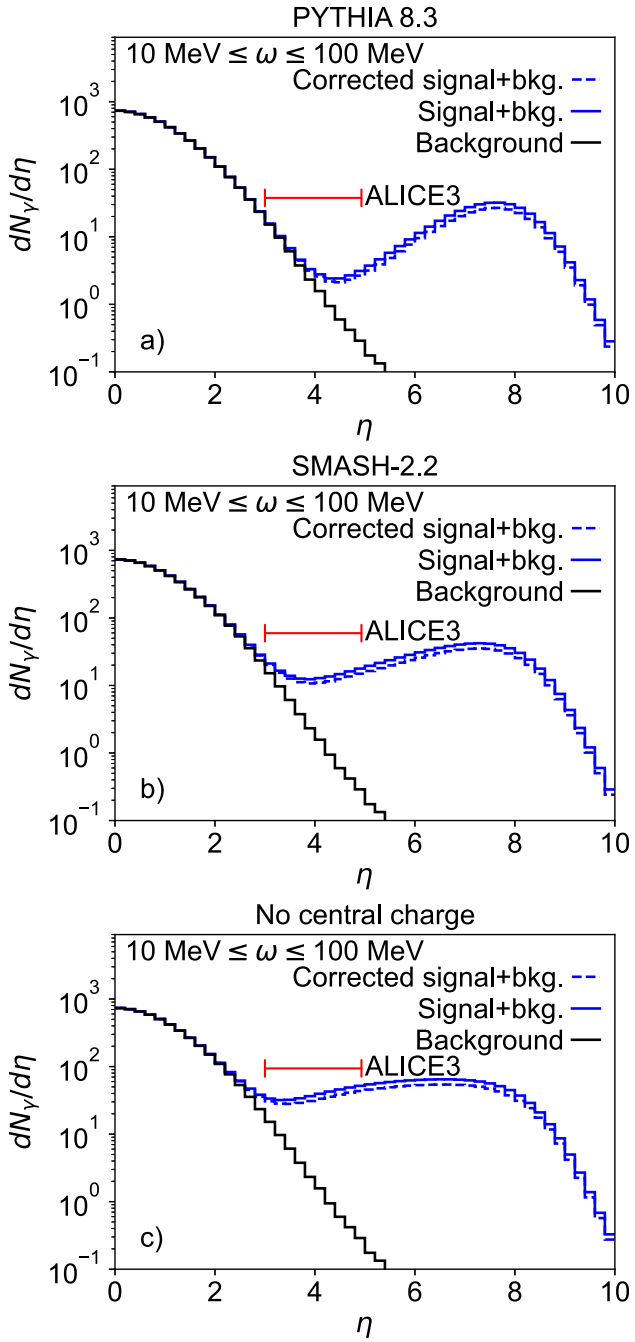

Fig. 4 Same as Fig. 3 but for photons in the energy range $0.01 \leq \omega \leq 0.1$ GeV

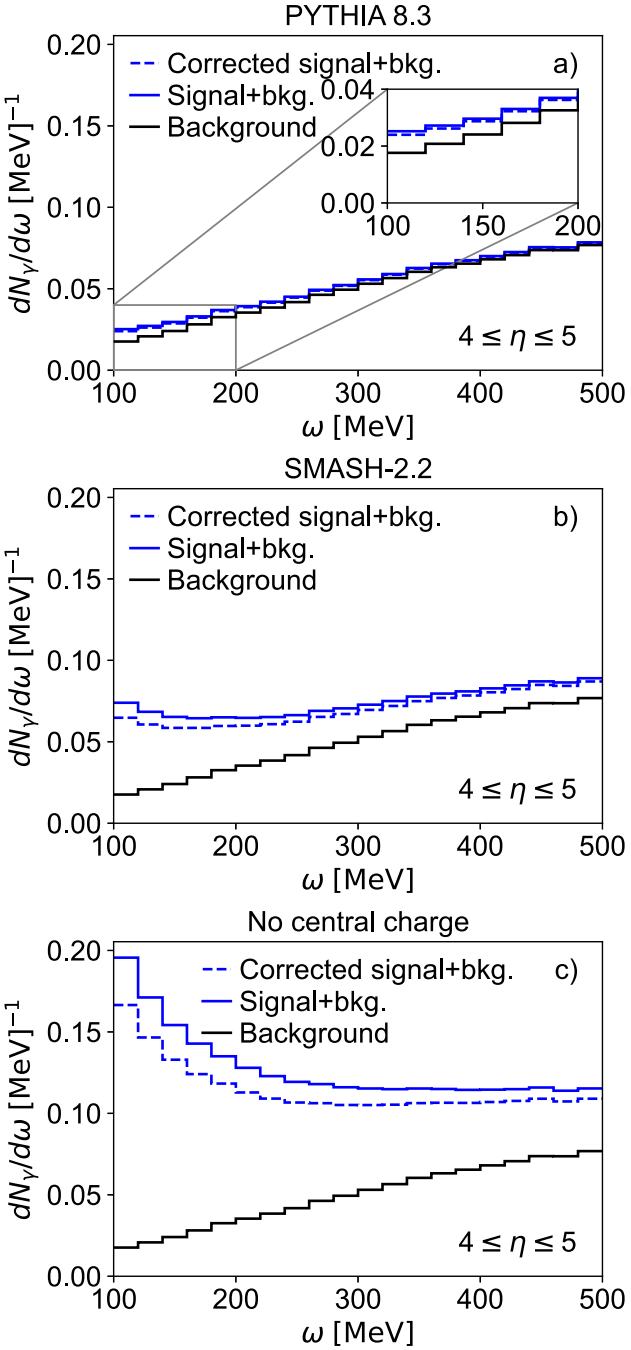

Fig. 5 The energy distributions for photons with $4.0 \leq \eta \leq 5.0$ integrated over the azimuthal angle. The black histogram shows the background from hadronically produced photons. The solid blue histogram shows the sum of the photons from bremsstrahlung radiation and hadronic production. The correction applied to the bremsstrahlung spectrum to obtain the dashed blue histogram is described in the text. The inset in a) shows the low energy region

background. The hadronic background should be well constrained from measurements of charged and neutral particle spectra.

4 Summary

To conclude, we have shown that even with realistic stopping scenarios the bremsstrahlung spectra show a strong sensitivity to the amount of nuclear stopping. Comparisons with Pythia show that a significant signal over the hadronic background is obtained in the range $\eta \gtrsim 4$–5 and $\omega \lesssim 300$–

500 MeV. Again, the exact limits depend on the amount of stopping one has.

Considering the importance of determining the amount of stopping in heavy-ion collisions at the LHC, and given that no alternative methods are available, we believe the possibility to use bremsstrahlung photons should be considered seriously. Hopefully this paper can help in the design of future detectors to accomplish such a measurement.

Acknowledgements We thank Hannah Elfner for providing the net proton distributions from SMASH-2.2. This work is supported by the Norwegian Research Council.

Data Availability Statement This manuscript has no associated data or the data will not be deposited. [Authors' comment: The results of our numerical studies can be obtained from the authors upon request.]

Funded by SCOAP[3]. SCOAP[3] supports the goals of the International Year of Basic Sciences for Sustainable Development.

References

1. B. Muller, J. Schukraft, B. Wyslouch, First results from Pb + Pb collisions at the LHC. Annu. Rev. Nucl. Part. Sci. **62**, 361–386 (2012). https://doi.org/10.1146/annurev-nucl-102711-094910. arXiv:1202.3233 [hep-ex]
2. S. Chatrchyan et al., Measurement of the pseudorapidity and centrality dependence of the transverse energy density in PbPb collisions at $\sqrt{s_{NN}}$ = 2.76 TeV. Phys. Rev. Lett. **109**, 152303 (2012). https://doi.org/10.1103/PhysRevLett.109.152303. arXiv:1205.2488 [nucl-ex]
3. J. Adam et al., Measurement of transverse energy at midrapidity in Pb–Pb collisions at $\sqrt{s_{\rm NN}}$ = 2.76 TeV. Phys. Rev. C **94**(3), 034903 (2016). https://doi.org/10.1103/PhysRevC.94.034903. arXiv:1603.04775 [nucl-ex]
4. A. Bazavov et al., Equation of state in (2 + 1)-flavor QCD. Phys. Rev. D **90**, 094503 (2014). https://doi.org/10.1103/PhysRevD.90.094503. arXiv:1407.6387 [hep-lat]
5. L. Adamczyk et al., Bulk properties of the medium produced in relativistic heavy-ion collisions from the beam energy scan program. Phys. Rev. C **96**(4), 044904 (2017). https://doi.org/10.1103/PhysRevC.96.044904. arXiv:1701.07065 [nucl-ex]
6. I.C. Arsene et al., Nuclear stopping and rapidity loss in Au + Au collisions at s(NN)**(1/2) = 62.4-GeV. Phys. Lett. B **677**, 267–271 (2009). https://doi.org/10.1016/j.physletb.2009.05.049. arXiv:0901.0872 [nucl-ex]
7. I.G. Bearden et al., Nuclear stopping in Au + Au collisions at s(NN)**(1/2) = 200-GeV. Phys. Rev. Lett. **93**, 102301 (2004). https://doi.org/10.1103/PhysRevLett.93.102301. arXiv:nucl-ex/0312023
8. H. Appelshauser et al., Baryon stopping and charged particle distributions in central Pb + Pb collisions at 158-GeV per nucleon. Phys. Rev. Lett. **82**, 2471–2475 (1999). https://doi.org/10.1103/PhysRevLett.82.2471. arXiv:nucl-ex/9810014
9. J. Mohs, S. Ryu, H. Elfner, Particle production via strings and baryon stopping within a hadronic transport approach. J. Phys. G **47**(6), 065101 (2020). https://doi.org/10.1088/1361-6471/ab7bd1. arXiv:1909.05586 [nucl-th]
10. M. Li, J.I. Kapusta, Large baryon densities achievable in high energy heavy ion collisions outside the central rapidity region. Phys. Rev. C **99**(1), 014906 (2019). https://doi.org/10.1103/PhysRevC.99.014906. arXiv:1808.05751 [nucl-th]
11. L.D. McLerran, S. Schlichting, S. Sen, Spacetime picture of baryon stopping in the color-glass condensate. Phys. Rev. D **99**(7), 074009 (2019). https://doi.org/10.1103/PhysRevD.99.074009. arXiv:1811.04089 [hep-ph]
12. B. Abelev et al., Pion, kaon, and proton production in central Pb–Pb collisions at $\sqrt{s_{NN}}$ = 2.76 TeV. Phys. Rev. Lett. **109**, 252301 (2012). https://doi.org/10.1103/PhysRevLett.109.252301. arXiv:1208.1974 [hep-ex]
13. B. Abelev et al., Centrality dependence of π, K, p production in Pb–Pb collisions at $\sqrt{s_{NN}}$ = 2.76 TeV. Phys. Rev. C **88**, 044910 (2013). https://doi.org/10.1103/PhysRevC.88.044910. arXiv:1303.0737 [hep-ex]
14. S. Acharya et al., Production of charged pions, kaons, and (anti-)protons in Pb–Pb and inelastic pp collisions at $\sqrt{s_{NN}}$ = 5.02 TeV. Phys. Rev. C **101**(4), 044907 (2020). https://doi.org/10.1103/PhysRevC.101.044907. arXiv:1910.07678 [nucl-ex]
15. J.I. Kapusta, Bremsstrahlung in the nuclear fireball model. Phys. Rev. C **15**, 1580–1582 (1977). https://doi.org/10.1103/PhysRevC.15.1580
16. J.D. Bjorken, L.D. McLerran, Coherent photon radiation from nuclei as a probe of impact parameter and nucleon velocity distribution in ultrarelativistic nuclear collisions. Phys. Rev. D **31**, 63 (1985). https://doi.org/10.1103/PhysRevD.31.63
17. A. Dumitru, L.D. McLerran, H. Stoecker, W. Greiner, Soft photons at RHIC and LHC. Phys. Lett. B **318**, 583–586 (1993). https://doi.org/10.1016/0370-2693(93)90457-S
18. S. Jeon, J.I. Kapusta, A. Chikanian, J. Sandweiss, Nucleus–nucleus bremsstrahlung from ultrarelativistic collisions. Phys. Rev. C **58**, 1666–1670 (1998). https://doi.org/10.1103/PhysRevC.58.1666. arXiv:nucl-th/9806047
19. J.I. Kapusta, S.M.H. Wong, Imaging the space-time evolution of high-energy nucleus–nucleus collisions with bremsstrahlung. Phys. Rev. C **59**, 3317 (1999). https://doi.org/10.1103/PhysRevC.59.3317. arXiv:hep-ph/9903235
20. S. Park, U.A. Wiedemann, Bremsstrahlung photons from stopping in heavy-ion collisions. Phys. Rev. C **104**(4), 044903 (2021). https://doi.org/10.1103/PhysRevC.104.044903. arXiv:2107.05129 [hep-ph]
21. J.D. Jackson, *Classical Electrodynamics* (Wiley, New York, 1975)
22. S. Park, Opportunities with ultra-soft photons: bremsstrahlung from stopping. (2022). arXiv:2208.01527 [hep-ph]
23. C. Bierlich et al., A comprehensive guide to the physics and usage of PYTHIA. SciPost Phys. Codebases **8**, 3 (2022). arXiv:2203.11601 [hep-ph]
24. S. Klein, J. Nystrand, Exclusive vector meson production in relativistic heavy ion collisions. Phys. Rev. C **60**, 014903 (1999). https://doi.org/10.1103/PhysRevC.60.014903. arXiv:hep-ph/9902259
25. C. Bierlich, G. Gustafson, L. Lönnblad, H. Shah, The Angantyr model for heavy-ion collisions in PYTHIA8. JHEP **10**, 134 (2018). https://doi.org/10.1007/JHEP10(2018)134. arXiv:1806.10820 [hep-ph]

26. J. Weil et al., Particle production and equilibrium properties within a new hadron transport approach for heavy-ion collisions. Phys. Rev. C **94**(5), 054905 (2016). https://doi.org/10.1103/PhysRevC.94.054905. arXiv:1606.06642 [nucl-th]
27. R. Aaij et al., LHCb detector performance. Int. J. Mod. Phys. A **30**(07), 1530022 (2015). https://doi.org/10.1142/S0217751X15300227. arXiv:1412.6352 [hep-ex]
28. M. Kłusek-Gawenda, R. McNulty, R. Schicker, A. Szczurek, Light-by-light scattering in ultraperipheral heavy-ion collisions at low diphoton masses. Phys. Rev. D **99**(9), 093013 (2019). https://doi.org/10.1103/PhysRevD.99.093013. arXiv:1904.01243 [hep-ph]
29. ALICE: letter of intent: a forward calorimeter (FoCal) in the ALICE experiment. CERN-LHCC-2020-009, LHCC-I-036 (2020)
30. ALICE: letter of intent for ALICE 3: A next generation heavy-ion experiment at the LHC, Geneva. CERN-LHCC-2022-009, LHCC-I-038 (2022)